JOURNAL OF CATALYSIS 150, 117–126 (1994)

Pumice-Supported Palladium Catalysts

I. Chemical Preparation and Microstructural Features

Giuliano Fagherazzi,* Alvise Benedetti,* Giulio Deganello,†,[1] Dario Duca,† Antonino Martorana,† and Giuseppe Spoto‡

*Dipartimento di Chimica Fisica, Università di Venezia, Calle Larga S. Marta 2137, 30123, Venezia; †Dipartimento di Chimica Inorganica, Università di Palermo, and Istituto di Chimica e Tecnologia dei Prodotti Naturali, CNR, Via Archirafi 26-28, 90123 Palermo; and ‡Dipartimento di Chimica Inorganica, Chimica Fisica e Chimica dei Materiali, Università di Torino, Via Giuria 7, 10125 Torino, Italy.

Received June 7, 1993; revised March 16, 1994

Two series of pumice-supported palladium catalysts (W = washed, U = unwashed) were prepared by the reaction of $[Pd(C_3H_5)_2]$ with the support, followed by reduction using H_2. W catalysts were washed before reduction to eliminate unreacted $[Pd(C_3H_5)_2]$. U catalysts did not undergo this treatment. Microstructural characterization of the catalysts was performed by small-angle X-ray scattering (SAXS), wide-angle X-ray line broadening, and transmission electron microscopy (TEM). Line-broadening analysis revealed the presence of lattice imperfections, such as growth stacking faults and microstrains in the fcc structure of palladium. The average particle size values determined by SAXS were confirmed by TEM analysis and were employed to calculate the percentage of palladium exposed (catalyst dispersion). W catalysts showed well-dispersed spheroidal particles, whereas the U series displayed agglomerates.

1. INTRODUCTION

Suitable supports for metallic catalysts are important in heterogeneous catalysis since they can modify the chemical reactivity and physical characteristics of the metal phase (1, 2). Indeed, microstructural features strongly affect the properties of heterogeneous catalysts (3–6).

Very small (nanometric) metal crystallites may be considered as intermediates between the single atom and the infinite atom arrays of the bulk metal (7). A great deal of progress has been made in understanding the correlations between geometry and chemistry with regard to the well-defined surface of a metal single crystal (8). However, these correlations are more intricate in the case of very finely dispersed metal crystallites or particles (5, 9–11) since they may depend on many factors, such as the type of metal, the particle size or the percentage of metal exposed (dispersion), possible metal–support interactions, as well as the specific chemical reaction being investigated.

Whereas a low metal concentration in supported catalysts is more suitable for industrial purposes, microstructural characterization of catalysts becomes more and more difficult as the metal content decreases. As far as X-ray scattering is concerned, a further bias is constituted by possible interferences between the metal particles and the support. In this respect, pumice, a natural aluminosilicate containing a high percentage of silica and, as its chief impurities, potassium and sodium (12) is an ideal amorphous support with a low specific surface (about 5 m^2/g, as determined by small angle X-ray scattering) and, consequently, very low microporosity. In fact, these pumice features minimize X-ray scattering interferences between the palladium nanometric particles and the support material, as has previously been shown (13, 14).

On the other hand, according to the Thiele modulus (15), the low specific surface of the support increases the efficiency coefficient of a supported metal catalyst. These characteristics actually minimize the effects of mass and heat transfer (16) connected with interparticle diffusion, so that, when other diffusional processes are not operative, a kinetic study of the catalyzed reaction can be performed on the basis of a "pure chemical regime."

Pumice as support could therefore become a model for laboratory reactions that are usually controlled by interparticle diffusion, whereas pumice-supported highly dispersed metal catalysts could be of interest in industrial processes in which intraparticle mass and heat transfers are important.

The use of pumice as a support (17) for metal catalysts is not widely documented, probably because of its poorly defined composition. However, we found that samples of pumice taken from various caves at Lipari (Italy) and treated with dilute HNO_3 had an almost constant composition and very similar physico-chemical features (12).

[1] To whom correspondence should be addressed.

0021-9517/94 $6.00

In this paper we report the chemical preparation of a series of pumice-supported palladium catalysts and their microstructural characterization, carried out by wide-angle line-broadening X-ray analysis (WAXS-LB), small-angle X-ray scattering (SAXS), and transmission electron microscopy (TEM).

2. EXPERIMENTAL PROCEDURES

All the reagents employed (Riedel-de-Haen or Aldrich) were of analytical grade. The solvents were dried and distilled from potassium in a nitrogen atmosphere before use. Their purity was tested by GC analysis. All reactions were performed in an inert atmosphere. $[Pd(C_3H_5)_2]$ was prepared according to published procedures (18). The pumice powder is waste from the building material manufactured (19) by Pumex S.p.A. at Lipari. Before use, it was treated as reported in Ref. (20).

2.1. Chemical Preparation of Catalysts

Palladium was supported following a procedure described by Yermakov (21). In a typical experiment, a pumice suspension in pentane (10 g in 50 ml) was treated at −10°C with a pentane solution of $[Pd(C_3H_5)_2]$ (22) of known concentration, in nitrogen. After about 30 min the suspension turned yellow-brown as a result of the anchoring reaction

$$\text{Pum-OH} + [Pd(C_3H_5)_2] \rightarrow C_3H_6 + \text{Pum-O-Pd}(C_3H_5)$$

where Pum = pumice support and OH = hydroxyl groups of pumice. The mixture was then stirred at 0°C for 1 h.

Reduction to metallic Pd was obtained using high-purity H_2 [provided by ISO S.p.A. of Palermo and passed through a BTS catalyst (Fluka) for removal of oxygen traces] for half an hour at −15°C. This low-temperature procedure minimizes the sintering of metal crystallites during the reduction of anchored $Pd(C_3H_5)$. The mixture was then kept at 0°C for 1 h (during which time hydrogen was stirred in) and at 25°C for half an hour. The solvent was evaporated under reduced pressure at 25°C. The catalyst was then vacuum-dried and stored at room temperature under nitrogen containing traces of oxygen. The catalysts passivated were then examined by SAXS, WAXS, and TEM.

Two different kinds of catalyst, listed in Table 1, were synthesized and employed. The two types differ because they underwent dissimilar treatment immediately before reduction: those marked with the letter "W" were gradually "washed" before reduction, by three subsequent substitutions of the solution with an equal amount of solvent; those marked with "U" did not receive this treatment. The different procedures were used in an attempt to compare the two types of catalyst: in the reduction of the "washed" catalysts, palladium atoms should come mainly from OH-anchored $Pd(C_3H_5)$, whereas in the "unwashed" catalysts metal atoms that are also produced from a $[Pd(C_3H_5)_2]$ solution may crystallize. The latter procedure is likely to promote the formation of metal particle agglomerates.

2.2. WAXS-LB and SAXS Analyses

We used a Philips vertical goniometer connected to a highly stabilized generator (Siemens Kristalloflex 805). Ni-filtered Cu$K\alpha$ radiation was employed and the diffracted beam was monochromatized with a focusing graphite monochromator (Bragg-Brentano geometry). We used a proportional counter and 0.05° step sizes in 2θ for an accumulated counting time of 100 s per angular abscissa.

Line-broadening (LB) analysis of the palladium reflections (indexed on the basis of the fcc unit cell with edge a_0 = 3.8898 Å) was performed by fitting pseudo-Voigt functions to the experimental peak profile intensities in accordance with previously reported procedures (23–25). Our methods adopt the Simplex modified algorithm (26) with a routine to determine parameter errors and correlations (27), and are tailored for running on a PC.

SAXS data were collected with a Paar compact Kratky camera, using Ni-filtered Cu$K\alpha$ radiation and a scintillator counter, with fixed 10^5 counts per angular abscissa.

2.3. TEM Analysis

The samples for TEM analyses were first dispersed in isopropyl alcohol and then supported on a copper grid coated with a holey carbon film. The TEM analyses were carried out on a Jeol JEM-2000EX transmission electron microscope equipped with a top entry stage. The micrographs were scanned with an image analyzer system (IBAS 2000 Kontron) to determine the diameter distributions of the palladium particles.

On micrographs taken under high-resolution conditions, many metal particles show interference fringes caused by recombination of the transmitted and diffracted beams. However, in view of (i) the presence of the amorphous matrix which strongly reduces image contrast, (ii) the limited number of fringes visible on the small particles on less concentrated samples, and (iii) the formation of aggregates (which produce Moiré fringes on more concentrated ones), it is very difficult to measure their spacing with sufficient accuracy and hence to unequivocally recognize the atomic planes involved.

3. OUTLINE OF THE WAXS AND SAXS METHODS AND THEORY

The "true" experimental background deriving from the pumice was taken into account in the fitting procedure

TABLE 1

Composition and Microstructural Parameters of the Palladium Catalysts Investigated[a]

Sample[b]	Pd[c] (wt%)	$\langle D\rangle_V$[d] (Å)	D_S^*[e] (Å)	$\langle D\rangle_{SAXS}$[f] (Å)	$\langle D\rangle_{TEM}$[g] (Å)	D_P[h] (Å)	S_{Sp}[i] (m^2/g)	D_X[i] (%)
U_2	0.27	n.d.	n.d.	45	n.d.	31	162	36
U_3	1.14	38(4)	36(8)	61	101	50	99	22
U_4	2.42	54(6)	48(9)	93	175	73	71	15
W_3	0.39	n.d.	n.d.	41	n.d.	35	142	32
W_4	0.61	27(4)	n.d.	49	49	35	142	32
W_5	0.86	35(6)	n.d.	53	n.d.	40	122	28

[a] The support with grain dimension >45 μm has a specific surface of about 2 m^2/g as determined by BET measurements; this value agrees with SAXS determination. The OH content of the pumice is about 5 ml H/g.

[b] U denotes unwashed catalysts, W washed ones.

[c] Determined with colorimetric method as reported in Ref. (22).

[d] Apparent volume-weighted average Pd crystallite diameters obtained by LB analysis of the (111) XRD peak [Eq. 2]. For sample U_4, both a $\langle D\rangle_V$ value of 63 Å and a microstrain content $[\langle\varepsilon^2_{L=20\text{ Å}}\rangle_{111}]^{1/2}$ of 0.0027 were determined by Warren–Averbach analysis on the (111)–(222) pair of XRD reflections [Eq. (1)].

[e] Apparent surface-weighted average Pd crystallite diameters obtained by LB analysis of all the (111), (200), (220), (311), and (222) peak profiles investigated according to the procedure explained in the text. The approach cannot be applied to catalysts with too low a metal content.

[f] Surface-weighted average Pd particles diameters determined by Titchmarsh transform.

[g] Surface-weighted average Pd particles diameters determined by automatic scanning of the TEM photographs.

[h] Porod diameters.

[i] Specific surface obtained from the Porod diameter and, respectively, dispersion. The estimated error on these parameters is ±10%.

when it was duly scaled, point by point, in each WAXS diffractogram of catalysts. The matching obtained with the observed intensities was satisfactory, revealing that the support and palladium scatterings are additive. This is shown in Fig. 1, which concisely records the diffractograms of catalysts U_4 and W_5 and that of pumice.

The optimized pseudo-Voigt functions relating to $K\alpha_1$ components were Fourier-transformed; instrumental broadening was then eliminated by means of a deconvolutive procedure worked out in the Fourier space [L(Å)-space], thereby obtaining the corrected Fourier transforms $A(L)$ as shown in Ref. (23). When the Warren–Averbach (W–A) method (28) is directly applied to $A(L)$, the crystallite size–strain separation can be performed only on the (111)–(222) pair of reflections of the catalyst containing the most palladium (U_4). See Benedetti *et al.* (29), which refers to a discussion on the use of W–A analysis when analytical fitted functions are adopted. On U_3, W_4, and W_5 samples, the weak (222) reflection [which, moreover, widely overlaps the (311) reflection] prevented us from using the two-line Fourier analysis; as a consequence, only the (111) reflection could be investigated.

In both procedures a volume-weighted average (apparent) crystallite size, $\langle D\rangle_V$, was determined. For catalyst U_4, to which the W–A analysis could be applied, $\langle D\rangle_V$ is given by

$$\langle D\rangle_V = \int_0^\infty L^2 \frac{d^2 A^S(L)}{dL^2}\, dL \qquad (1)$$

where $A^S(L)$ are the crystallite size components of the $A(L)$ Fourier transforms as determined by the W–A method. For catalysts U_3, W_4, and W_5, to which the single-line analysis was applied, $\langle D\rangle_V$ is directly given by

$$\langle D\rangle_V = \int_0^\infty L^2 \frac{d^2 A(L)}{dL^2}\, dL \qquad (2)$$

since in this case, following the initial slope approximation of Nandi *et al.* (30), the unknown $A^S(L)$ Fourier components are approximated by the known $A(L)$ Fourier transforms.

As reported by Fagherazzi *et al.* (13), some reflections [especially the (200) reflection] are slightly but clearly asymmetrical and shifted in comparison with the angular positions of a pure Pd reference sample. This was attributed to the presence of a nonnegligible amount of stacking faults. However, for the purposes of this paper, in which

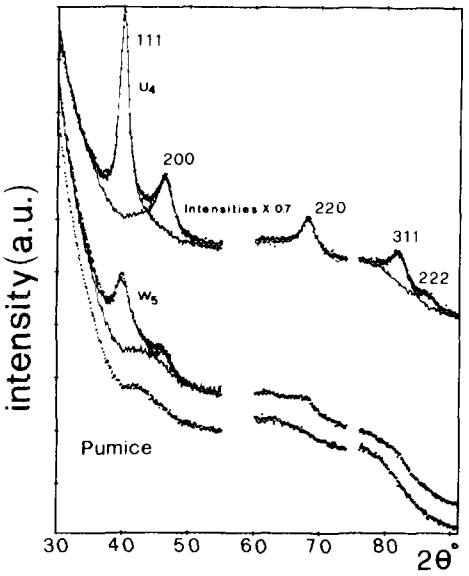

FIG. 1. X-ray diffractograms (in compact form) of catalysts U_4 and W_5 and of pumice (background). The continuous curves represent the sums of the matched experimental background with the optimized pseudo-Voigt functions. For graphic reasons the experimental intensities were plotted at a step size of 0.10° instead of 0.05°, and the background was not indicated beneath the catalyst diffractograms. Only the first two (111) and (200) peaks could be fitted for sample W_5.

only LB is investigated, all peaks were considered symmetrical, thus simplifying the best-fitting procedure.

Using the simplified single-line approach, we only attributed the LB to small crystallite sizes. To investigate the possible presence of stacking faults in the Pd lattice by LB, an apparent average surface-weighted crystallite size D_S (*hkl*), in the [*hkl*] crystallographic direction, was also determined according to the equation (28)

$$\left[\frac{dA(L)}{dL}\right]_{L\to 0} = -\frac{1}{D_S(hkl)}. \tag{3}$$

As discussed by Nandi *et al.* (30), this simplified single-line LB analysis is justified when the broadening caused by microstrains is much lower than that due to crystallite size, so that the former can be neglected. In fact, if the microstrain values of all catalysts investigated resemble those found in U_4 (see Table 1) with the W–A method, the contribution to LB due to crystallite size should be widely predominant. Moreover, it is reasonable to assume that, in this type of material, microstrains are homogeneously distributed in all crystallographic directions, so that, when they are neglected, nearly equivalent underestimations of the apparent crystallite size should occur, whatever *hkl* reflection is considered.

On the basis of the above approximations, we attempted to determine the influence of stacking faults on $D_S(hkl)$ by employing the following simplified equation, which does not include microstrain broadening effects (31):

$$\frac{1}{D_S(hkl)} = \frac{1}{D_S^*} + \frac{(1.5\alpha + \beta)}{a_0} V(hkl). \tag{4}$$

Here D_S^* is the average "true" surface-weighted crystallite size taken as a constant for all crystallographic directions (hypothesis of equiassic crystallites, substantially confirmed by TEM in this particular case; $\alpha = \alpha' + \alpha''$ is the total deformation stacking fault probability, the sum of single (α') and double (α'') deformation probabilities; β is the growth or twin stacking fault probability; and $V(hkl)$ is a parameter dependent on the *hkl* reflection. $V(hkl)$ values are recorded in Table 7.1 of Ref. (31). When, by plotting $[D_S(hkl)]^{-1}$ vs $V(hkl)$, a linear trend is recognizable, D_S^* and $1.5\alpha + \beta$ can be obtained following Eq. (4).

Owing to the low surface area of the support and the high metal dispersion observed, the SAXS signal of palladium particles could be subtracted from the total scattering of the catalyst, after scaling had been carried out. In this way we were able to draw the Porod $J(h)h^3$ vs h^3 plot, where $J(h)$ is the slit-smeared intensity arising from the

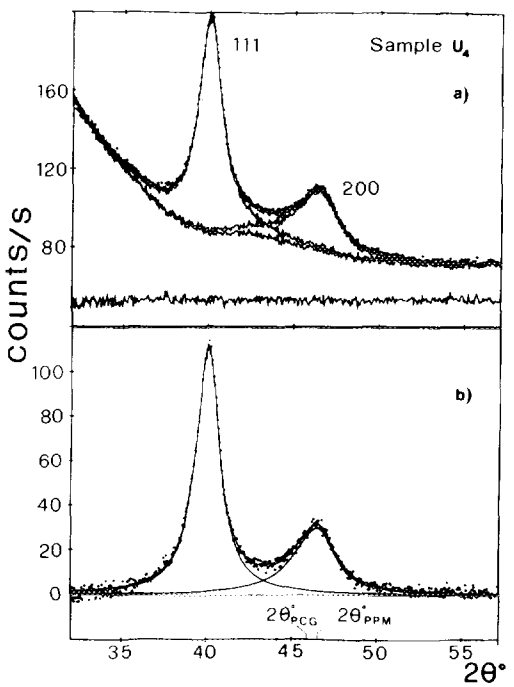

FIG. 2. (111) and (200) fitted peak profiles. (a) The continuous curves represent the sums of the matched experimental background with optimized pseudo-Voigt asymmetric functions. (b) Where the background was subtracted, the asymmetry of the (200) peak can be estimated at the bottom of the figure from the difference between the baricenter position $2\theta_{PCG}$ and the peak maximum position $2\theta_{PPM}$.

TABLE 2

Stacking Fault Probabilities for Catalysts U_3 and U_4

Sample	From peak shift $\alpha = \alpha' - \alpha''$	From peak asymmetry $\beta + 4.5\alpha''$	From LB $1.5(\alpha' + \alpha'') + \beta$
U_3	n.d.[a]	0.03(1)	0.08(4)
U_4	0.0015(4)	0.05(1)	0.16(8)

[a] The relative weakness of the peaks of this sample (1.14% of Pd) did not enable a reliable determination of this parameter from the peak shift.

metal phase and h is equal to $4\pi \sin(\theta)/\lambda$, where λ is the radiation wavelength.

For the equations used to determine the specific surface S_{Sp} of the metal phase as well as the Porod average diameter D_P (32) of the palladium particles (assumed spherically shaped), we refer to Polizzi *et al.* (33). The Porod diameters were converted to the percentage of metallic atoms exposed, D_X, on the basis of the published values (34) concerning the numbers of surface palladium atoms per polycrystalline surface unit area by means of the expression $D_X(\%) = [11.2/D_P(\text{Å})] \times 100$. In the hypothesis of spherically shaped particles, the diameter distribution functions and the relative average diameters were obtained using the Titchmarsh transform according to the theoretical approach suggested by Fedorova and Schmidt (35). To provide a closer comparison with the Porod diameter D_P, which is a surface-weighted mean (36), SAXS TEM size distributions as well as were surface-weighted.

4. RESULTS AND DISCUSSION

As explained in Ref. (13), the (200) peak shown in Fig. 2 for catalyst U_4, in which the fitting of the (111)–(200) peak envelope was performed with asymmetrical profile functions, is shifted toward smaller 2θ's. From the difference between $2\theta^\circ_{PPM}$ (peak maximum position) and

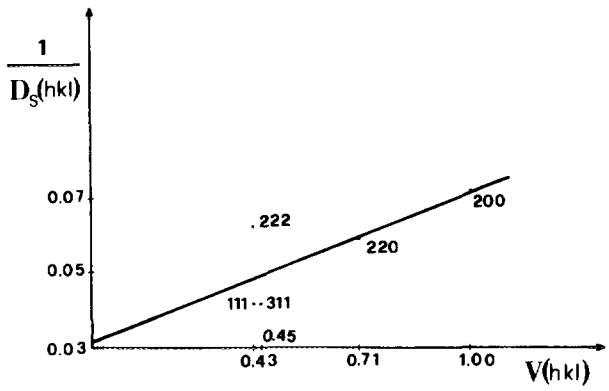

FIG. 3. Plot of $D_S^{-1}(hkl)$ vs $V(hkl)$ for catalyst U_4.

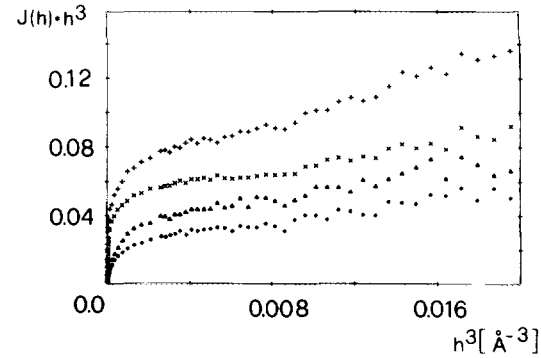

FIG. 4. Porod $J(h)h^3$ vs h^3 plots for catalysts U_2 (◆), W_3 (▲), U_3 (x), and U_4 (+). The scattering caused by pumice was duly subtracted.

$2\theta^\circ_{PCG}$ (peak center of gravity), the stacking fault probability could be calculated for sample U_4. The relevant value is reported in the first column of Table 2.

Table 1 records the values obtained for $\langle D\rangle_V$ and D_S^* for the more loaded metal catalysts since the WAXS peaks for the remaining ones (U_2 and W_3) were too weak to be correctly analyzed. It is interesting to note that the value of $[\langle \varepsilon^2_{L=20\,\text{Å}}\rangle_{111}]^{1/2}$ found for sample U_4 (0.0027) is very similar to that found by Nandi *et al.* (37) in silica-supported Pd catalysts. On the other hand, Pielaszek (38) detected larger amounts (about 0.007) of microstrains in Pd catalysts supported on γ-alumina. Figure 3 shows the $[D_S(hkl)]^{-1}$ vs $V(hkl)$ plots relative to the U_4 catalyst from which the overall stacking faults probabilities and the "true" D_S^* average particle size were determined. Table 2 records the values of the diversely determined stacking fault probabilities, including those already reported elsewhere on the same samples (13) as obtained by asymmetry and peak shift analysis. A comparison of these values shows that the stacking fault probabilities calculated by LB are higher than those previously published. On the other hand, the present values are closer to those previously calculated for these two catalysts on the basis of a structural model allowing for growth faults in the sequence of Pd layers, as well as for size distri-

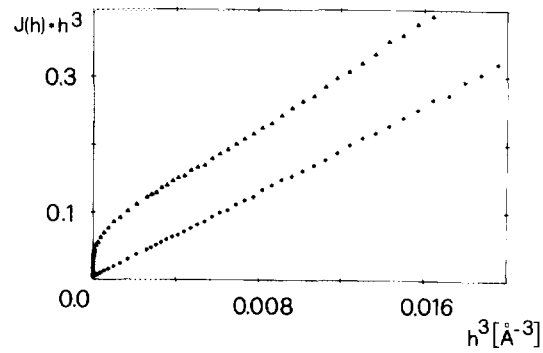

FIG. 5. Porod $J(h)h^3$ vs h^3 plots for pumice (◆) and U_4 (▲).

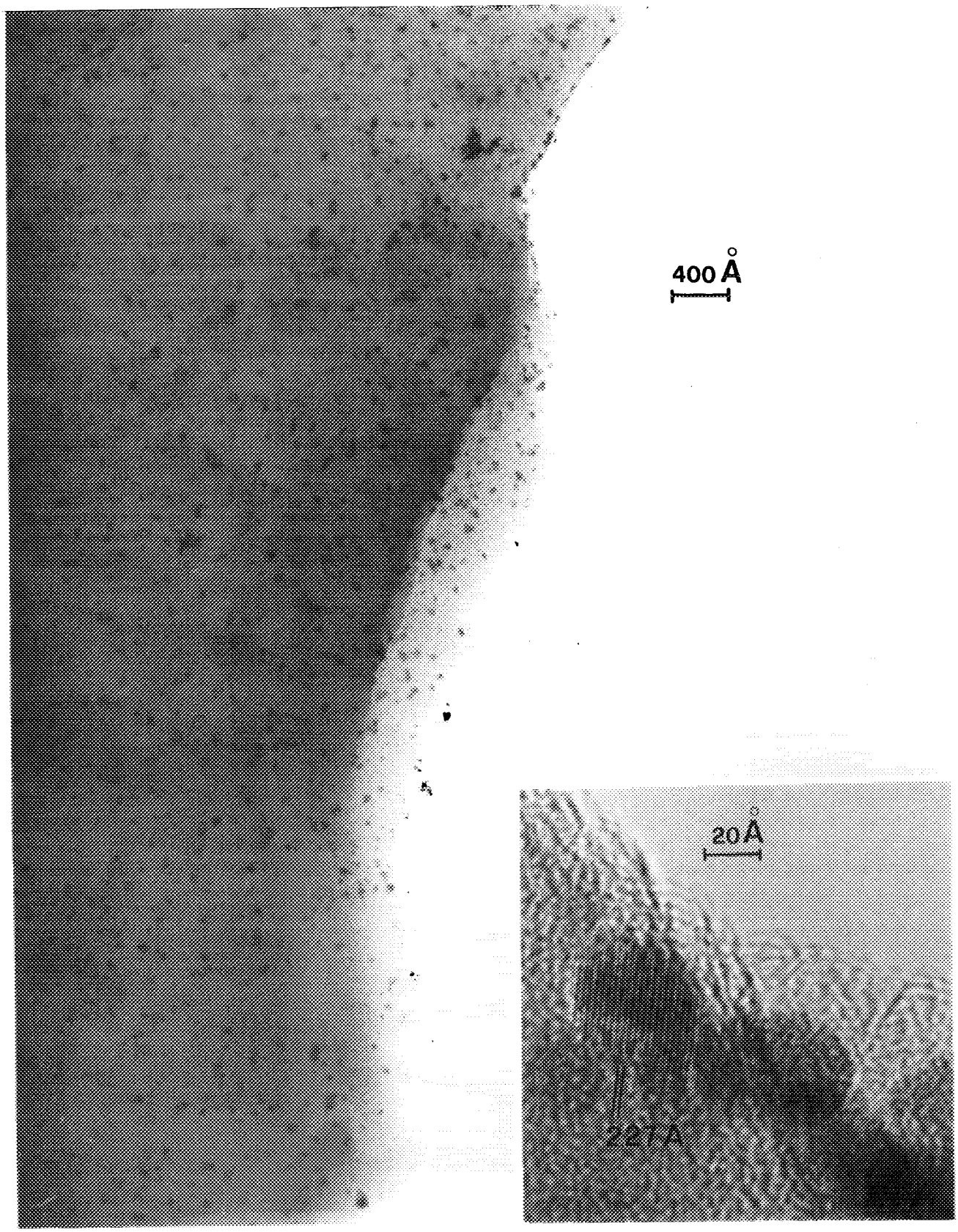

FIG. 6. Transmission electron micrograph of catalyst W_4. The inset gives an enlarged view of some metal particles: Pd(111) planes are resolved.

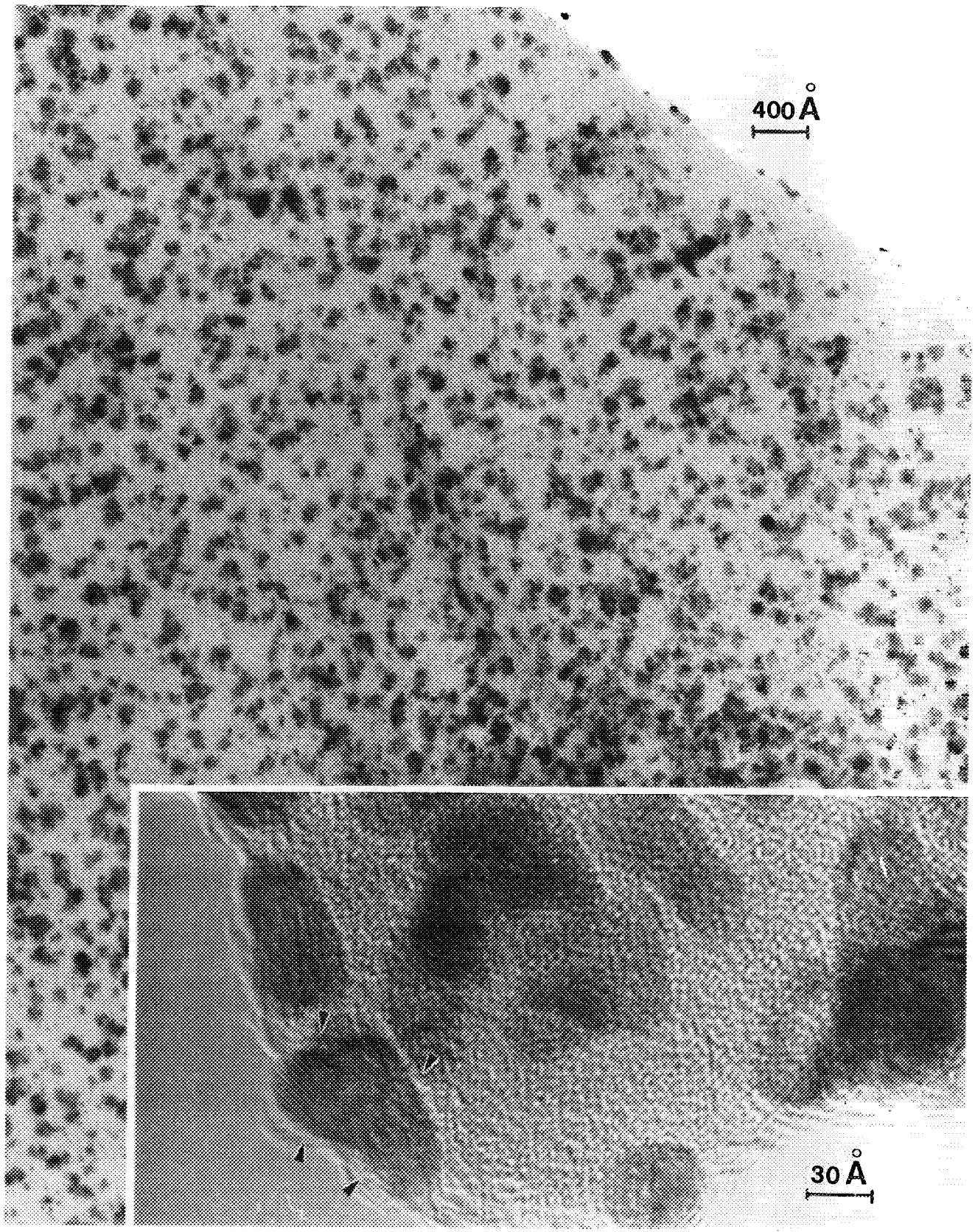

FIG. 7. Transmission electron micrograph of catalyst U_3. In the high-resolution image (inset), arrows indicate abrupt changes in the direction of atomic planes.

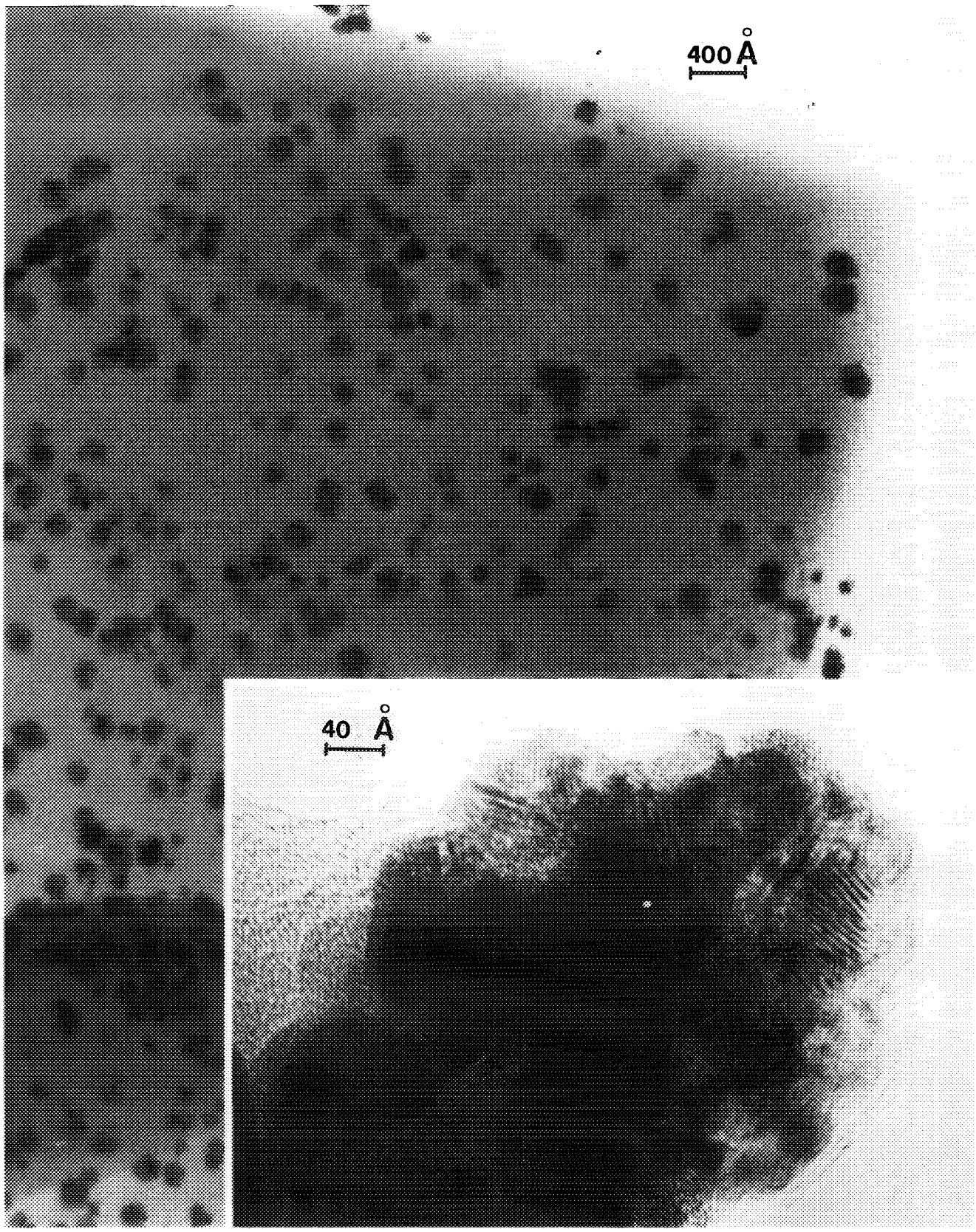

FIG. 8. Transmission electron micrograph of catalyst U_4. The inset shows a large aggregate of Pd particles under high-resolution conditions.

bution and disorder of the second kind within the metal crystallites (14).

In Fig. 4 Porod plots are drawn for four of the six catalysts investigated by means of SAXS (the other two, which are not reported for graphic reasons, are similar), after the scattering due to the pumice support has been subtracted. Figure 5 shows the Porod plots for pumice and the U_4 catalyst. Table 1 illustrates all the WAXS and SAXS results on crystallite and particle sizes (assumed spherically shaped), on specific surfaces and dispersions, obtained according to the definitions and methods described in the previous section.

The average particle sizes found by SAXS, which are systematically but not remarkably higher than the corresponding sizes found by WAXS-LB, were substantially confirmed by TEM observation. Figures 6, 7, and 8 show the micrographs for W_4, U_3, and U_4 samples, respectively. The W_4 sample shows well-dispersed equiassic or spheroidal particles with sizes in the range centered around 30–50 Å; for U_3, the range is about 40–80 Å and some agglomerates are detectable; finally, U_4 shows several agglomerates, whose indented borders suggest that they are composed of heaps of individual particles of 70–100 Å. Figure 9 compares the surface-weighted diameter distributions obtained by SAXS and TEM for catalyst W_4. From the results reported in Table 1 it can be concluded that the agreement between the two techniques is good as long as the catalysts are well dispersed (both SAXS and TEM "see" the particles). In the more loaded catalysts, on the contrary, due to the presence of aggregates of particles, the agreement is no longer that good (TEM hardly distinguishes the single particles in the aggregate) and, as expected, the $\langle D \rangle_{TEM}$ values are higher than the $\langle D \rangle_{SAXS}$ values.

It is worth noting (see, for example, the inset in the TEM micrograph in Fig. 7) that, in some cases, abrupt changes in the direction of the fringes could point to the presence of twinned crystals, probably associated with growth stacking faults. It is important to note that the TEM micrograph of a washed catalyst containing 1.75 wt% Pd (not reported in Table 1, $D_P = 50$ Å, $S_{Sp} = 100\ m^2/g$ of Pd) showed several widespread particles and only a few agglomerates, from which the effectiveness of the washing process in improving dispersion could be inferred. This catalyst was reused in the hydrogenation at 25°C of a THF solution (2.5×10^{-1} *M*) of 1,3-cyclooctadiene, for 5 h (five times higher concentration than in the other experiments reported in the succeeding Part II of this work). SAXS analysis of this reused catalyst gave $D_P = 61$ Å and $S_{Sp} = 82\ m^2/g$ Pd, showing that the pumice-supported palladium catalysts were fairly stable with regard to sintering effects.

5. CONCLUSIONS

Palladium catalysts supported on pumice were prepared according to Yermakov's procedure with a metal concentration ranging between about 0.3 and 2.4 wt%. Fairly highly dispersed metal phases were obtained in both series of "unwashed" and "washed" samples.

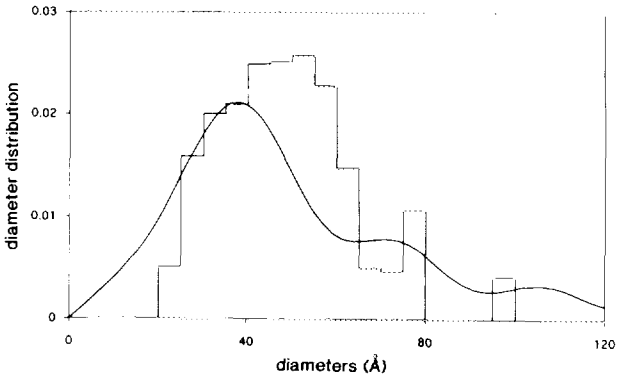

FIG. 9. SAXS (continuous line) and TEM (histogram-like) surface-weighted size distributions of sample W_4.

Lattice microstrains and stacking faults were detected and measured in the fcc palladium structure by means of WAXS-LB Fourier analysis. The amount of microstrains thus determined tallies with published data concerning silica-supported palladium catalysts (37), and the presence of stacking faults already evidenced by us (13) was confirmed. The amount of growth stacking faults determined here is close to that found by means of a fitting procedure based on a specific palladium stacking model (14). These structural features could be linked to an interaction between the support material and the dispersed metal phase or to the actual growth process of metal crystallites which, on the contrary, could be independent of the support material.

The particle size values measured by SAXS were substantially confirmed by TEM. Percentages of palladium exposed, D_X, were calculated starting from the average Porod diameters. These are used in the next paper (Part II) to determine turnover frequencies in the first and second hydrogenations of 1,3-cyclooctadiene, carried out in liquid phase. SAXS measurements revealed a moderate sintering of metal particles in a catalyst reused under drastic conditions in the hydrogenation of the 1,3-cyclooctadiene to cyclooctene.

ACKNOWLEDGMENTS

We are grateful to Professor A. Zecchina of the University of Turin for his useful criticism and helpful discussion and to Dr. M. Battagliarin and Mr. L. Bertoldo for their assistance in the X-ray diffraction data analysis.

We thank CNR (Progetto Finalizzato Materiali Speciali per le Tecnologie Avanzante and Progetto Finalizzato Chimica Fine II) and the Ministero dell'Università e della Ricerca Scientifica (MURST 40%) for their financial support, and Pumex S.p.A. for supplying pumice samples and awarding a grant to one of us (D.D.).

REFERENCES

1. Tamaru, K., "Dynamic Heterogeneous Catalysis." Academic Press, London, 1978.
2. Ehrburger, P., and Walker, P. L., Jr., *J. Catal.* **55,** 63 (1978).
3. Bond, G. C., *Surf. Sci.* **156,** 966 (1978).
4. Burch, R., *Catalysis (London)* **7,** 149 (1985).
5. Anderson, J. R., *Sci. Prog. (Oxford)* **69,** 461 (1985).
6. Somorjai, G. A., *Science* **227,** 902 (1985).
7. Howard, J. A., and Mile, B., *Acc. Chem. Res.* **20,** 173 (1987).
8. Somorjai, G. A., "Chemistry in Two Dimensions, Surface." Cornell University, Ithaca, NY, 1981.
9. Boudart, M., *Adv. Catal.* **20,** 153 (1969).
10. Anderson, J. R., "Structure of Metallic Catalysts." Academic Press, London, 1975.
11. Farin, D., and Avnir D., *J. Am. Chem. Soc.* **110,** 2039 (1988).
12. Venezia, A. M., Floriano, M. A., Deganello, G., and Rossi, A., *Surf. Interface Anal.* **18,** 619 (1992).
13. Fagherazzi, G., Benedetti, A. Martorana, A., Giuliano, S., Duca, D., and Deganello, G., *Catal. Lett.* **6,** 263 (1990).
14. Martorana, A., Deganello, G., Duca, D., Benedetti, A., and Fagherazzi, G., *J. Appl. Crystallogr.* **25,** 31 (1992).
15. Gut, G., Kut, O. M., Yuecelen, F., and Wagner, D., *in* "Catalytic Hydrogenation" (Červeny, L., Ed.), p. 517. Elsevier, Amsterdam, 1986
16. Ruiz, P., Criné, M., Germain, A., and L'Homme, G., *in* "Chemical and Catalytic Reactor Modelling" (M. P. Dudukovic and P. L. Mills, Eds.), p. 15. ACS Symposium Series 237. Am. Chem. Soc., Washington, DC, 1984.
17. Boutonnet, M., Kizling, J., Mintsa-Eya, V., Choplin, A., Touroude, R., Maire, G, and Stenius, P., *J. Catal.* **103,** 95 (1987).
18. Jolly, P. W., *Angew. Chem. Int. Ed.* **24,** 283 (1985).
19. Luca, S. F., "La Pomice di Lipari," Technical Bulletin. Pumex, Messina, 1986.
20. Brunauer, S., and Emmett, P. H., *J. Am. Chem. Soc.* **59,** 2682 (1937).
21. Yermakov, Y. I., *Catal. Rev.* **13,** 77 (1986).
22. Yoe, J. H., and Kirkland, J. J., *Anal. Chem.* **26,** 1335 (1954).
23. Enzo, S., Polizzi, S., and Benedetti, A., *Z. Kristallogr.* **170,** 275 (1985).
24. Enzo, S., Fagherazzi, G., Benedetti, A., and Polizzi, S., *J. Appl. Crystallogr.* **21,** 536 (1988).
25. Polizzi, S., Fagherazzi, G., Benedetti, A., Battagliarin, M., and Asano T., *J. Appl. Crystallogr.* **23,** 359 (1990).
26. Nelder, J. A., and Mead, R., *Comput. J.* **7,** 308 (1965).
27. Press, W. H., Flannery, B. P., Teukilsky, S. A., and Vetterling, W. T., "Numerical Recipes," p. 521. Cambridge Univ. Press, New York, 1986.
28. Warren, B. E., "X-Ray Diffraction," p. 264. Addison–Wesley, Reading, MA, 1969.
29. Benedetti, A., Fagherazzi, G., Enzo, S., and Battagliarin, M., *J. Appl. Crystallogr.* **21,** 543 (1988).
30. Nandi, R. K., Kuo, H. K., Schlosberg, W., Wisser, G., Cohen, J. B., and Crist, B., Jr., *J. Appl. Crystallogr.* **17,** 22 (1984).
31. Wagner, C. N. J., *in* "Local Atomic Arrangements Studies by X-Ray Diffraction" (J. B. Cohen and J. E. Hilliard, Eds.), p. 219. Gordon & Breach, New York, 1966.
32. Porod, G., *in* "Small Angle X-ray Scattering" (O. Glatter and O. Kratky, Eds.), p. 17. Academic Press, London, 1982.
33. Polizzi, S., Benedetti, A., Fagherazzi, G., Franceschin, S., Goatin, C., Talamini, G., and Toniolo, L., *J. Catal.* **106,** 483 (1987).
34. Anderson, J. R., "Structure of Metallic Catalysts," p. 296. Academic Press, London, 1975.
35. Fedorova, I. S., and Schmidt, P. W., *J. Appl. Crystallogr.* **11,** 405 (1978).
36. Whyte, T. E., Jr., Kirklin, P. W., Gould R.W., and Heinemann, H., *J. Catal.* **25,** 407 (1972).
37. Nandi, R. K., Pitchai, R., Wong, S. S., Cohen, J. B., Burwell, R. L., Jr., and Butt, J. B., *J. Catal.* **70,** 298 (1981).
38. Pielaszek, J., *Catal. Lett.* **1,** 117 (1988).